Three-Level Space Vector PWM in Low Index Modulation Region Avoiding Narrow Pulse Problem

Hyo L. Liu and Gyu H. Cho

Abstract—**In using GTO, a few hundreds micro seconds longer than specified pulse width must be guaranteed for safety for each device to commutate with its inherent gate current sequences. This paper describes the mechanism of generating undesirable narrow pulses in conventional three-level space vector PWM and suggests two new algorithms of space vector PWM using Non-Nearest three and four vectors in a control period to avoid such a narrow pulse problem. Experimental verifications for the suggested algorithms are also presented.**

I. Introduction

THE three-level inverter topology is being widely used in high voltage/high power applications due to its high voltage handling and good harmonic rejection capabilities with currently available power devices like GTO's. Fig. 1 shows the basic circuit diagram of three-level inverter excluding detailed snubber circuits and antiparallel diodes. It is known that the three-level inverter roughly improves by a factor of four the harmonics content compared with conventional two-level topology having the same number of devices and ratings.

So far various PWM techniques controlling three-level inverter have been studied and a good plenty of results are published such as modified two-level triangular carrier modulation, cost function minimizing PWM and space vector PWM [1]–[3].

Among these, the space vector PWM is often preferred not only in the low modulation index region but also in the middle and high modulation index regions. The reason is due to its simplicity both in hardware and software and innate real time PWM capability which is essential for some applications such as field oriented induction motor control.

Especially the space vector PWM exhibits relatively good performance in the low modulation index region which we are concerned within this paper compared with the other PWM methods. The main superiorities are

1) coping well with frequently varying fundamental to switching frequency ratio,
2) simple hardware and software compared with other programmed strategies which are complex due to the vast amount of angle data,
3) asynchronous PWM is possible which is useful in the low frequency region.

Conventional space vector PWM strategy with **NTV** selection law using the closest three vectors to command, however, is not adequate in the low modulation index region because it generates narrow gating pulses. There are several important factors which must be considered in designing PWM method: i) available maximum device switching frequency, ii) harmonics content such as Total Harmonic Distortion (THD), iii) allowed Minimum Pulse Width (MPW), and iv) operating range. Among these, minimum pulse width is especially one of the most critical factors in GTO inverter because the on- and off-pulse widths must exceed at least a hundred microseconds in order for the GTO to commutate with special gate current sequences.

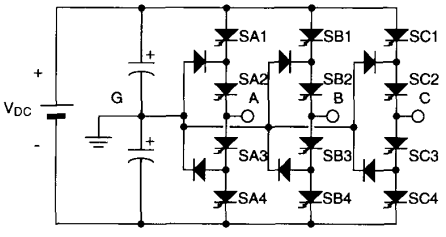

Fig. 1. Three-level inverter topology excluding antiparallel diodes.

The minimum pulse width becomes problematic as inverter frequency closes to either minimum or maximum. This is because dwell time at nonzero and zero vector becomes too narrow when the inverter frequency reaches either boundary value when constant voltage/frequency control is used.

The narrow pulse width problem has a close relation to starting performance. Solving this problem by ignoring pulse widths under a specified limit results in severe distorted output at low frequency, which means improper flux build up in the motor, resulting in low starting torque. Raising the starting frequency to avoid narrow pulses may cause large surge current hazardous to switches. So the method that does not generate narrow pulses at low frequency is desired.

In this paper the detailed mechanism of generation of narrow gating pulses in conventional **NTV** space vector PWM is described and new Non-Nearest Three and Four Vectors ($\mathbf{N^2TV}$ and $\mathbf{N^2FV}$) selection laws are suggested to avoid such narrow pulse problems. The experimental results are also presented.

II. Narrow Pulse Problem in Conventional Space Vector PWM with Nearest Three-Vector (NTV) Selection Law

Fig. 2 shows all space vectors of three-level inverter represented on d-q domain normalized by $2/3^*V_{DC}$. It is obtained by d-q transforming the output voltage of inverter made by various switch combinations. +, 0, and − represent the

Manuscript received May 14, 1993; revised March 25, 1994.

The authors are with the Department of Electrical Engineering, Korea Advanced Institute of Science and Technology, 373-1, Kusong Dong, Yusung Gu, Taejon, 305-701, Korea.

IEEE Log Number 9404433.

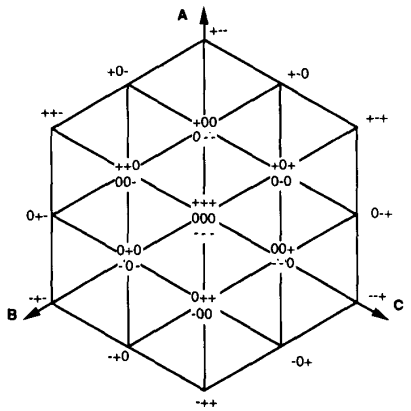

Fig. 2. Space vectors of three-level inverter.

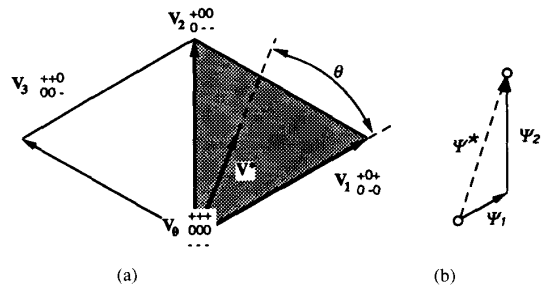

(a) (b)

Fig. 3. (a) Space vector PWM with Nearest Three-Vector selection law and (b) pseudo-flux trajectory between two arbitrary points.

possible output terminal voltages of the inverter shown in Fig. 1, respectively, $+V_{\rm dc}/2$, 0, and $-V_{\rm dc}/2$ if G is the reference. The space vector PWM is a PWM method that makes pseudo-flux have circular trajectory as far as possible, where the pseudo-flux is defined by

$$\psi = \int \boldsymbol{V} dt. \tag{1}$$

From now on, let us confine our discussion to PWM method only in the low modulation index less than 0.5(pu). The output frequency is also low when constant frequency/voltage ratio operation is used. In this case the modulation index, m, is defined by

$$m(\text{pu}) = \frac{|\boldsymbol{V}_o|}{2/3 \cdot V_{\rm DC}} \tag{2}$$

where $\boldsymbol{V}_o$: output voltage vector $V_{\rm dc}$: dc-link voltage. Fig. 3(a) shows the inner part of Fig. 2 explaining the algorithm of conventional NTV space vector PWM at certain instant. The voltage command $\boldsymbol{V}^*$ is rotating vector with magnitude of m and angular velocity of ω given by

$$\boldsymbol{V}^* = m \cdot \exp(j\omega t) = m \cdot \exp(j\theta). \tag{3}$$

Thus the $\boldsymbol{V}^*$ can fall in any triangle of Fig. 2 if the constant voltage/frequency method is used. Fig. 3(a) is a situation when $\boldsymbol{V}^*$ falls in a triangle made by $\boldsymbol{V}_0$, $\boldsymbol{V}_1$, and $\boldsymbol{V}_2$ which are voltage vector having magnitudes of 0, 0.5, and 0.5,

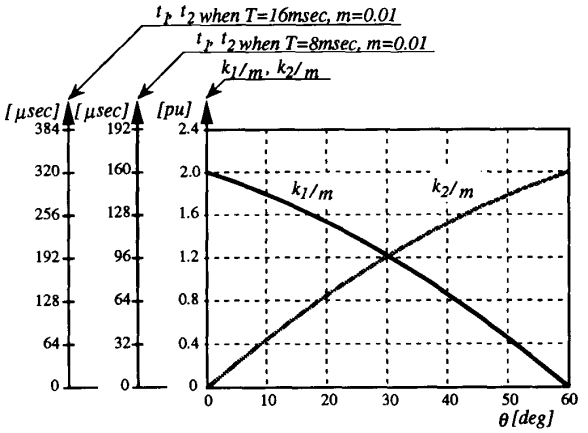

Fig. 4. Normalized duty ratios for $0° \leq \theta < 60°$ using Nearest Three-Vector selection law.

respectively. The command vector $\boldsymbol{V}^*$ is approximated for time interval T with following equations:

$$\boldsymbol{V}^* = k_1 \cdot \boldsymbol{V}_1 + k_2 \cdot \boldsymbol{V}_2 \tag{4}$$

$$1 = k_0 + k_1 + k_2 \tag{5}$$

$$[t_0, t_1, t_2] = T \cdot [k_0, k_1, k_2] \tag{6}$$

where k_0, k_1, and k_2 are the duty ratios of $\boldsymbol{V}_0$, $\boldsymbol{V}_1$, and $\boldsymbol{V}_2$, respectively, and t_0 , t_1, t_2 are the corresponding dwell times for the period T. In this case, the vector sequence is $\boldsymbol{V}_0[000]-\boldsymbol{V}_1[0-0]-\boldsymbol{V}_2[+00]$ for natural point voltage control [3] and the pseudo-flux trajectory between two arbitrary points is shown in Fig. 3(b). It seems nice because the pseudo-flux trajectory is much closed to the straight line passing the two points but there exist unallowed narrow pulses. Rewriting (4),

$$\begin{bmatrix} V_d^* \\ V_q^* \end{bmatrix} = \begin{bmatrix} V_{d1} & V_{d2} \\ V_{q1} & V_{q2} \end{bmatrix} \begin{bmatrix} k_1 \\ k_2 \end{bmatrix} \tag{7}$$

$$\begin{bmatrix} m \cdot \cos\theta \\ m \cdot \sin\theta \end{bmatrix} = \begin{bmatrix} 0.5 & 0.5 \cdot \cos 60° \\ 0 & 0.5 \cdot \sin 60° \end{bmatrix} \begin{bmatrix} k_1 \\ k_2 \end{bmatrix}, 0° \leq \theta < 60°. \tag{8}$$

Therefore,

$$\begin{bmatrix} \frac{k_1}{m} \\ \frac{k_2}{m} \end{bmatrix} = \begin{bmatrix} 0.5 & 0.5 \cdot \cos 60° \\ 0 & 0.5 \cdot \sin 60° \end{bmatrix}^{-1} \begin{bmatrix} \cos\theta \\ \sin\theta \end{bmatrix}, 0° \leq \theta < 60°. \tag{9}$$

Fig. 4 shows k_1/m and k_2/m obtained from (9) for $0° \leq \theta < 60°$. This is repeated every 60° as θ increases. k_1/m and k_2/m approach zero when θ becomes close to 0° and 60°, respectively. If $m = 0.01$ then, about one half of all θ's belong to the region where the dwell time is less than 100 μs when $T = 8$ μs, and quarter of θ's belong to this region when $T = 16$ μs. In order to maintain the minimum pulse width longer than a specified time interval, T must be taken as large as possible and the dwell time below that interval should be ignored. However, this approach forces under utilization of maximum available switching frequency of the devices and increases flux and torque ripples significantly.

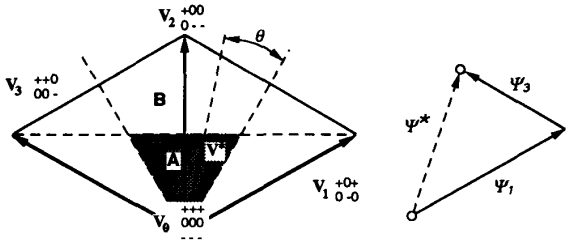

Fig. 5. (a) Space vector PWM with Non-Nearest Three-Vector selection law and (b) pseudo-flux trajectory between two arbitrary points.

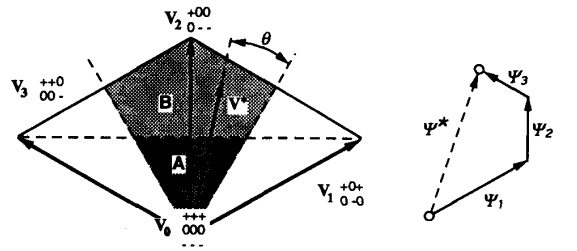

Fig. 7. (a) Space vector PWM with Non-Nearest Four-Vector selection law and (b) pseudo-flux trajectory between two arbitrary points.

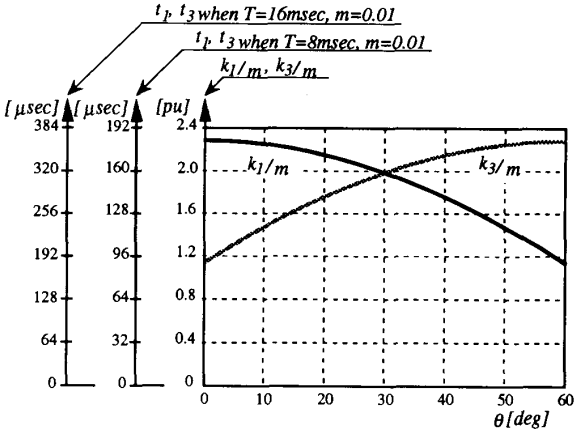

Fig. 6. Normalized duty ratios for $0° \leq \theta < 60°$ using Non-Nearest Three-Vector selection law.

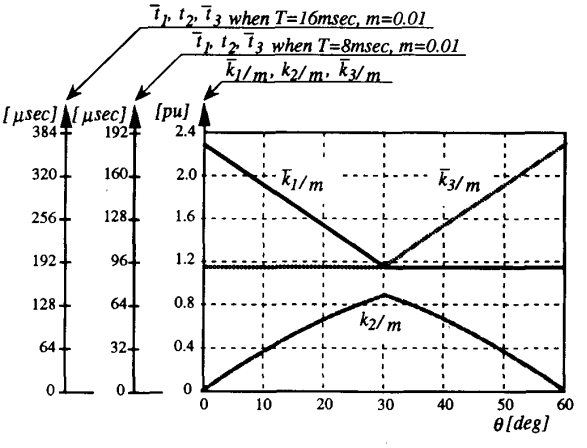

Fig. 8. Normalized duty ratios for using Non-Nearest Four-Vector selection law.

III. Suggested Space Vector PWM: Non-Nearest Three-Vector (N^2TV) Selection Law

Very sharp pulses are generated using the **NTV** law in the low modulation index region because the nearest vectors are selected to approximate $\boldsymbol{V}^*$. If some vectors far from the command vector $\boldsymbol{V}^*$ are selected, their duty ratio is longer. The authors suggest a space new vector PWM using an **N^2TV** selection law which uses the voltage vectors $\boldsymbol{V}_1$ and $\boldsymbol{V}_3$ further away from the command vector $\boldsymbol{V}^*$ than the $\boldsymbol{V}_1$ and $\boldsymbol{V}_2$ used in **NTV**, as shown in Fig. 5(a). In this case the command vector $\boldsymbol{V}^*$ in region $\boldsymbol{A}$ can be approximated by the following relations like in **NTV**:

$$\boldsymbol{V}^* = k_1 \cdot \boldsymbol{V}_1 + k_3 \cdot \boldsymbol{V}_3 \tag{10}$$

$$1 = k_0 + k_1 + k_3 \tag{11}$$

$$[t_0, t_1, t_3] = T \cdot [k_0, k_1, k_3]. \tag{12}$$

Rewriting (10),

$$\begin{bmatrix} V_d^* \\ V_q^* \end{bmatrix} = \begin{bmatrix} V_{d1} & V_{d3} \\ V_{q1} & V_{q3} \end{bmatrix} \begin{bmatrix} k_1 \\ k_3 \end{bmatrix} \tag{13}$$

$$\begin{bmatrix} m \cdot \cos\theta \\ m \cdot \sin\theta \end{bmatrix} = \begin{bmatrix} 0.5 \cdot \cos(-30°) & 0 \\ 0.5 \cdot \sin(-30°) & 0.5 \end{bmatrix} \begin{bmatrix} k_1 \\ k_3 \end{bmatrix}, 0° \leq \theta < 60°. \tag{14}$$

Thus,

$$\begin{bmatrix} \frac{k_1}{m} \\ \frac{k_3}{m} \end{bmatrix} = \begin{bmatrix} 0.5 \cdot \cos(-30°) & 0 \\ 0.5 \cdot \sin(-30°) & 0.5 \end{bmatrix}^{-1} \begin{bmatrix} \cos\theta \\ \sin\theta \end{bmatrix}, 0° \leq \theta < 60°. \tag{15}$$

If we consider the vector sequence as $\boldsymbol{V}_0[000] - \boldsymbol{V}_1[+0+] - \boldsymbol{V}_3[++0]$, then the pseudo-flux trajectory is the one shown in Fig. 5(b). The k_1/m and k_3/m factors do not approach zero when θ approaches 0° and 60°, respectively. The minimum period T can be obtained from the following inequality without losing controllability for all θ

$$T_{\min} \geq \frac{MPW}{m \cdot (k/m)_{\theta=0°,60°}} = \frac{MPW}{m \cdot 1.155}. \tag{16}$$

For example, if $m = 0.01$ and the specified $MPW = 100$ μs, then the condition $T_{\min} \geq 8.66$ ms guarantees the pulse width greater than 100 μs for any of the pulses in **N^2TV**.

Although the output harmonics seem to be somewhat increased due to the selection of nonnearest vectors, they can be made smaller than for the **NTV** law because a much smaller period T can be used.

IV. Modified N^2TV Method: Non-Nearest Four-Vector (N^2FV) Selection Law

With the **N^2TV** method described previously, only the $\boldsymbol{V}^*$ in region $\boldsymbol{A}$ [in Fig. 7(a)] can be approximated. This is understandable considering that the center of mass of plate $\boldsymbol{A}$ cannot be placed outside region $\boldsymbol{A}$. So, additional $\boldsymbol{V}_2$ vector

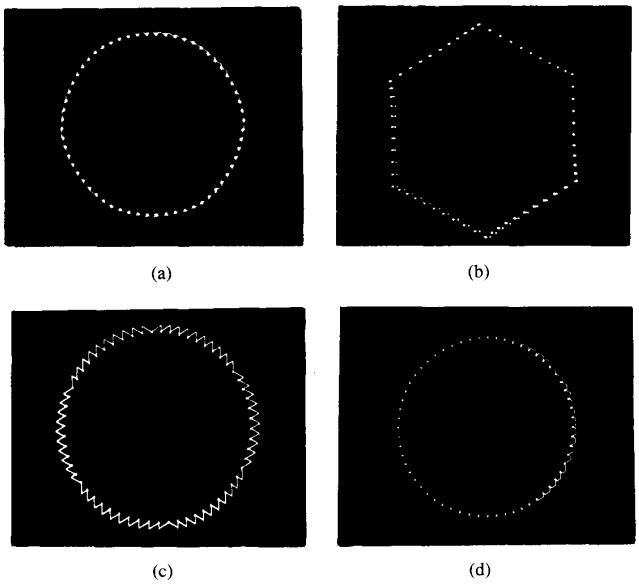

Fig. 9. Pseudo flux trajectories when $f_O = 2.5$ Hz, $m = 0.05$, and $T = 6.67$ ms, by (a) Nearest Three-Vector selection law allowing narrow pulses, (b) Nearest Three-Vector selection law ignoring narrow pulses under 100 μs, (c) Non-Nearest Three-Vector selection law, (d) Non-Nearest Four-Vector selection law.

must be included between $\boldsymbol{V}_1$ and $\boldsymbol{V}_3$. We call this method the Non-Nearest Four-Vector ($\mathbf{N^2FV}$) selection law covering both $\boldsymbol{A}$ and $\boldsymbol{B}$ region. The pseudo-flux trajectory is shown in Fig. 7(b) in period T. We can see without proof that the flux ripple is somewhat reduced compared to $\mathbf{N^2TV}$ [Fig. 5(b)] by introducing one more vector close to $\boldsymbol{V}^*$. Now we have the following equations relating the four vectors:

$$\boldsymbol{V}^* = k_1 \cdot \boldsymbol{V}_1 + k_2 \cdot \boldsymbol{V}_2 + k_3 \cdot \boldsymbol{V}_3 \tag{17}$$

$$1 = k_0 + k_1 + k_2 + k_3 \tag{18}$$

$$[t_0, t_1, t_2, t_3] = T \cdot [k_0, k_1, k_2, k_3]. \tag{19}$$

There exist many solutions satisfying the above equations because there are four unknown variables and only three equations [two in (17) and one in (18)]. On the other hand, considering that k_2 should be taken as large as possible in order to reduce the output harmonics satisfying $\min(t_1, t_3) \geq MPW$, then, k_2 is defined by

$$\begin{aligned} k_2/m &= \min(k_1/m, k_3/m) - (k/m)_{\theta=0^\circ,60^\circ} \\ &= \min(k_1/m, k_3/m) - 1.155 \end{aligned} \tag{20}$$

where,

$$\min(A, B) = \left\{ \begin{matrix} A, \text{if } A \geq B \\ B, \text{if } < B \end{matrix} \right\}.$$

With the relation of

$$\boldsymbol{V}_2 = \boldsymbol{V}_1 + \boldsymbol{V}_3, \tag{21}$$

the modified duty ratio $\bar{k}_1/m$ and $\bar{k}_3/m$ are obtained as

$$\bar{k}_1/m = k_1/m - k_2/m \tag{22}$$

$$\bar{k}_3/m = k_3/m - k_2/m. \tag{23}$$

Now, we have

$$\boldsymbol{V}^* = \bar{k}_1 \cdot \boldsymbol{V}_1 + k_2 \cdot \boldsymbol{V}_2 + \bar{k}_3 \cdot \boldsymbol{V}_3 \tag{24}$$

$$1 = k_0 + \bar{k}_1 + k_2 + \bar{k}_3 \tag{25}$$

$$[t_0, \bar{t}_1, t_2, \bar{t}_3] = T \cdot [k_0, \bar{k}_1, k_2, \bar{k}_3] \tag{26}$$

where $\bar{k}_1/m$, k_2/m, and $\bar{k}_3/m$ for $0^\circ \leq \theta < 60^\circ$ are shown in Fig. 8. Because $\boldsymbol{V}_2$ is inserted in a way that $\boldsymbol{V}_0[000] - \boldsymbol{V}_1[+0+] - \boldsymbol{V}_2[+00] - \boldsymbol{V}_3[++0]$, even small k_2 is not problematic. It is worth noting that $\mathbf{N^2FV}$ does not increase the switching frequency compared with $\mathbf{N^2TV}$ by introducing $\boldsymbol{V}_2$.

V. Experimental Results

To verify the validity of the proposed $\mathbf{N^2TV}$ and $\mathbf{N^2FV}$ algorithm, we tested these methods with real time three-level simulated inverter and 10 KVA transistor inverter being controlled by Motorola digital signal processor, DSP56000. The simulated inverter consists of several OP amps and offers various quantities of three-level inverter such as pole voltages (V_{AG}, V_{BG}, V_{CG} where, $\boldsymbol{G}$ is same as in Fig. 1), line to line voltages (V_{AB}, V_{BC}, V_{CA}), d-q component of output voltages (V_d, V_q) and pseudo-flux trajectories (Ψ_d, Ψ_q). We can see space vector of Fig. 2 and pseudo-flux trajectories using oscilloscope with X-Y display mode. The simulated inverter serves as very useful tool by preventing power circuit from being destroyed by erroneous control operation during debug process. The controller debugged by simulated inverter may then be applied to real power system.

Figs. 9 and 10 are experimental results with output frequency $f_o = 2.5$ Hz, $m = 0.05$, and $T = 6.67$ ms. Figs. 9(a) and (b) are pseudo-flux trajectories by $\mathbf{NTV}$ algorithm: (a) is obtained when allowing even narrow pulses

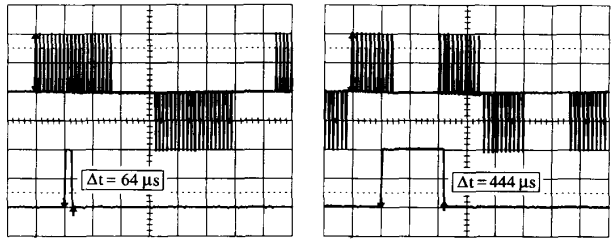

(a) (b)

Fig. 10. Line voltage (to G in Fig. 1) comparing pulse widths (upper) and their magnification along time axis (lower) by (a) Nearest Three-Vector selection law allowing narrow pulses, (b) Non-Nearest Four-Vector selection law.

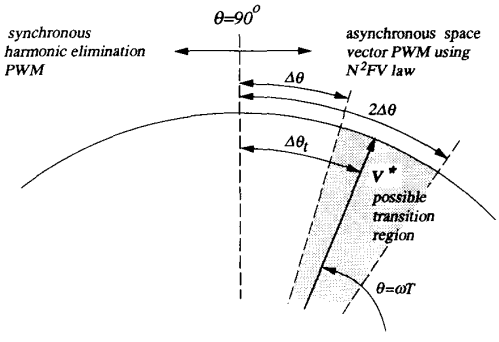

Fig. 11. Transition form asynchronous space vector PWM using Non-Nearest Four-Vector selection law to synchronous harmonic elimination strategy.

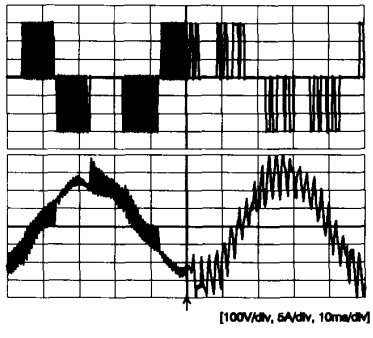

Fig. 12. Line voltage (to G in Fig. 1) of inverter (upper) and current (lower) during transition from asynchronous space vector PWM using Non-Nearest Four-Vector selection law to synchronous harmonic elimination strategy showing smooth transition.

and cannot be used in real situation whereas (b) is obtained when pulses having width under 100 μs are ignored, showing much distortion. Fig. 9(c) is that of $\mathbf{N^2TV}$ and shows somewhat large excursion around the command but has no narrow pulses under 100 μs. Whereas, Fig. 9(d) is obtained by $\mathbf{N^2FV}$ and shows much reduced excursion compared with $\mathbf{N^2TV}$ without generating narrow pulses. Fig. 10 displays the oscillodiagrams of the line voltage which is one of V_{AG}, V_{BG}, and V_{CG} (upper trace) and its magnification (lower trace) along the time axis in order to compare minimum pulse width of two algorithms. The voltage waveforms of Fig. 10(b) have some third harmonic component, but balanced load in three-phase system cannot see this. The minimum pulse width was 64 μs in $\mathbf{NTV}$ whereas 444 μs in $\mathbf{N^2FV}$.

In the higher modulation index region, the programmed synchronous PWM strategies such as *harmonic elimination and optimal* PWM are recommended because of their good harmonic quality and efficiency. At transition from one strategy to another, there must be no discontinuity both in magnitude of fundamental component and phase angle so as to reduce abnormal current spikes. The transition must occur when $\theta = 0°, 30°, 60°, \ldots, 270°$ in order not to violate symmetry of synchronous PWM. Fig. 11 shows one transition from asynchronous $\mathbf{N^2FV}$ to synchronous harmonic elimination PWM when $\theta = 90°$. Once transition is determined, the asynchronous $\mathbf{N^2FV}$ continues until θ is in possible transition region shown in the figure. At turning period, θ is jumped to 90° position with new time period $T_t = \frac{\Delta\theta_t}{\omega}$. This method makes no problem because T_t is in the range of $T \leq T_t < 2T$. After this, the harmonic elimination pattern follows subsequently. Experimental result of Fig. 12 shows the smooth transition with arrow indicating transition point.

VI. Conclusion

The detailed mechanisms of generating narrow pulses critical to GTO devices for conventional three-level space vector in the low modulation index region are explained. In this paper we suggested a new space vector PWM method guaranteeing minimum pulse width to overcome specified operation limit named as $\mathbf{N^2TV}$ and $\mathbf{N^2FV}$ selection law. The experimental results show that the $\mathbf{N^2FV}$ has the narrow pulse rejection capability.

References

[1] J. Holtz and L. Springob, "Reduced harmonics PWM controlled line-side converter for electric drives," *IEEE IAS*, pp. 959–964, 1990.
[2] T. Maruyama, M. Kumano, and M. Ashiya, "A new asynchronous PWM method for a three-level inverter," *IEEE PESC*, pp. 366–370, 1991.
[3] H. L. Liu , N. S. Choi, and G. H. Cho, "DSP based space vector PWM for three-level inverter with DC-link voltage balancing," *IEEE ICON*, pp. 197–201, 1991.

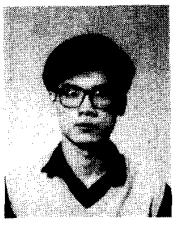

Hyo L. Liu was born in Chungnam, Korea, on May 2, 1966. He received the B.S. degree in electronic engineering from Hanyang University, in 1989, and the M.S. degree in electrical and electronic engineering from Korea Advanced Institute of Science and Technology (KAIST) in 1989.

He is presently a candidate for a doctor's degree. His field of interests are PWM of conventional and three-level inverters, three-phase ac-to-dc rectifier, static VAR compensator, and microprocessor-based control systems.

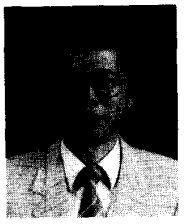

Gyu H. Cho was born in Korea on April 19, 1953. He received the M.S. and Ph.D. degrees from Korea Advanced Institute of Science and Technology (KAIST), Seoul, Korea, in 1977 and 1981, respectively.

From 1982 to 1983 he was with the Electronic Technology Division of the Westinghouse R&D Center, Pittsburgh, PA, where he worked on unrestricted frequency changer systems and inverters. Since 1984 he has been a Professor in the Department of Electrical Engineering of KAIST. His research interests are in the area of static power converters and devices, resonant converters, and integrated linear electronic-circuit design.